



**HAL**  
open science

# Efficient numerical integration of an elastic–plastic damage law within a mixed velocity–pressure formulation

R. El Khaoulani, Pierre-Olivier Bouchard

► **To cite this version:**

R. El Khaoulani, Pierre-Olivier Bouchard. Efficient numerical integration of an elastic–plastic damage law within a mixed velocity–pressure formulation. *Mathematics and Computers in Simulation*, 2013, 94, pp.145-158. 10.1016/j.matcom.2013.06.004 . hal-03605099

**HAL Id: hal-03605099**

**<https://minesparis-psl.hal.science/hal-03605099>**

Submitted on 10 Mar 2022

**HAL** is a multi-disciplinary open access archive for the deposit and dissemination of scientific research documents, whether they are published or not. The documents may come from teaching and research institutions in France or abroad, or from public or private research centers.

L'archive ouverte pluridisciplinaire **HAL**, est destinée au dépôt et à la diffusion de documents scientifiques de niveau recherche, publiés ou non, émanant des établissements d'enseignement et de recherche français ou étrangers, des laboratoires publics ou privés.

# Efficient numerical integration of an elastic-plastic damage law within a mixed velocity-pressure formulation

R. El khaoulani, P.-O. Bouchard

Mines ParisTech, CEMEF - Centre de Mise en Forme des Matériaux, CNRS UMR 7635,  
BP 207, 1 rue Claude Daunesse, 06904 Sophia Antipolis Cedex, France

---

## Abstract

This study focuses on numerical integration of constitutive law in numerical modeling of cold materials processing involving large plastic strain together with ductile damage. A mixed velocity-pressure formulation is used to handle the incompressibility of plastic deformation. A Lemaitre damage model where dissipative phenomena are coupled is considered. Numerical aspects of the constitutive equations are addressed in details. Three integration algorithms with different levels of coupling of damage with elastic-plastic behavior are presented and discussed in terms of accuracy and computational cost. The implicit gradient formulation with a non-local damage variable is used to regularize the localization phenomenon and thus to ensure the objectivity of numerical results for damage prediction problems. Tensile test on a plane plate specimen, where damage and plastic strain tend to localize in well-known shear bands, shows successfully both objectivity and effectiveness of the developed approach.

*Keywords: numerical integration of constitutive law; Ductile damage; numerical coupling; consistent tangent matrix; mixed finite element method; stabilized discretization  $P^{1+}/P^1$*

---

## 1 Introduction

Numerical modeling of cold metal forming processes has to account for large plastic strain together with the progressive degradation of material's properties. This degradation, induced by large plastic deformations, is commonly known as ductile damage phenomenon. The prediction of ductile damage growth and macro-crack initiation are essential issues in these numerical modelings. The Lemaitre ductile damage model [17, 18], where the damage and the plastic strain, i.e. dissipative phenomena, are coupled, has proven its effectiveness to deal with such applications. In this paper, an elastic-plastic damage constitutive law wherein the damage evolution obeys to this damage model is adopted.

Another important point, regarding large deformation modeling and ductile damage failure by the finite element method, is the nearly incompressible behavior, which is due to plastic

deformations incompressibility. The finite element approximation along with a reduced mechanical problem formulation might lead to severe volumetric locking phenomenon, thus unphysical pressure oscillations might occur [1, 9]. To handle the near incompressibility in elastic-plastic deformations, several strategies have been developed [8, 10, 25]. In this study a mixed variational formulation involving velocity and pressure fields together with a stabilized  $P^{1+}/P^1$  finite element discretization are considered. This stabilized finite element has been used in computational fluid mechanics for incompressible flows [14] and has been extended successfully to the problem of incompressibility observed in solid mechanics [7].

Efficiency of numerical integration of the constitutive equations has a direct impact on the overall efficiency of the finite element approximation. This is particularly true when dealing with complex constitutive models, such as elastic-plastic damage laws. The numerical way of coupling damage with the mechanical behavior can affect both accuracy and computational cost. In this context, we present here three integration algorithms with different levels of coupling of damage and plastic deformation within a mixed velocity-pressure formulation. These levels of coupling have been developed to find a better compromise between accuracy, computational cost, and implementation's simplicity for approaching equations of the constitutive law. These numerical aspects, which are related to local integration of an elastic-plastic damage constitutive law within a mixed velocity-pressure formulation, are the fundamental contributions of the present work.

Finite element approximation of problems involving damage leads to numerical results that heavily depend on the size and orientation of the mesh elements [12, 21, 24, 26]. Lots of solutions have been proposed to restore numerical modelings' objectivity of the finite element approach [2, 4, 13, 15, 19, 20, 23, 28]. Among these regularizing methods, the non-local damage theory based on a spatial smoothing of damage variable is widely used [2, 5, 6, 20]. In this study we consider the non-local damage model derived from the implicit gradient formulation.

The paper is structured as follows: first the adopted theoretical modeling of the constitutive law with ductile damage as well as the formulation of the mechanical problem in the mixed formulation are shortly presented in section 2. Numerical integration of constitutive equations and levels of coupling are treated in section 3. The non-local implicit formulation is shortly recalled in section 4. Finally, some numerical results are presented in section 5, which compare the effect of the different levels of coupling considered here and illustrate the effectiveness of the developed approach in damage prediction problems.

## 2 Theoretical modeling

Fractographic observations show that large plastic strains may bring about microscopic structural change of the material during the loading process. This evolution of microstructure includes micro-cracks and micro-voids nucleation, growth and coalescence leading to materials' softening. As a result, the macroscopic behavior of the structure is affected by these microscopic degradations.

Material degradation is modeled here using an elastic-plastic damage constitutive law that is based on the phenomenological approach. This approach is built at the macroscopic level by introducing internal variables to represent the microstructural phenomena. In particular, a damage variable is used to reflect materials' deterioration in their behavior.

## 2.1 Damage modeling

Damage variable, which is associated with material degradation, is defined as the ratio of the area of micro-voids and micro-cracks to the material's overall area [17]. Besides, it is assumed that the damaging process is isotropic and the scalar damage variable  $w$  represents the loss of structure stiffness. This variable is defined by the following stress-strain relationship [17]:

$$\sigma = (1 - w)\mathbb{C} : \varepsilon^e \quad (1)$$

where  $\mathbb{C}$  is the elastic constitutive tensor,  $\sigma$  the stress tensor and  $\varepsilon^e$  the elastic part of the strain tensor. Damage variable  $w$  varies from 0 for a sound material to 1 for a completely damaged material.

The evolution of damage obeys to a *Lemaitre* model [17]. The damage rate is considered as a function of both the damage strain energy release rate  $Y$  given by (3) and the equivalent strain rate  $\dot{\bar{\varepsilon}}$  as follows:

$$\dot{w} = \dot{\bar{\varepsilon}} \left( \frac{-Y}{s_0} \right)^b \delta_{\{\bar{\varepsilon} \geq \bar{\varepsilon}_d\}} \quad \delta_{\{\bar{\varepsilon} \geq \bar{\varepsilon}_d\}} = \begin{cases} 1 & \text{if } \bar{\varepsilon} \geq \bar{\varepsilon}_d \\ 0 & \text{if } \bar{\varepsilon} < \bar{\varepsilon}_d \end{cases} \quad 0 \leq w < w_c \text{ or } w = 1 \quad (2)$$

where  $s_0$  and  $b$  are material parameters,  $\bar{\varepsilon}_d$  is the critical value of accumulated plastic strain  $\bar{\varepsilon}$  from which the micro-cracks and micro-voids begin to have an impact on material response.  $w_c$  is a critical damage value which corresponds to macroscopic crack initiation, i.e. the macroscopic crack appears when  $w = w_c$ .

The expression of the damage strain energy release rate is given by [17]:

$$Y = \frac{-1}{2E(1-w)^2} [(1+\nu)\sigma : \sigma - \nu \text{tr}\sigma^2] \quad (3)$$

where  $\nu$  is the Poisson's ratio, and  $E$  is the Young's modulus.

## 2.2 Elastic-plastic damage law

An elastic-plastic model together with isotropic hardening and *von Mises* stress criterion are assumed in this work. Using the spherical/deviator decomposition of second-order tensors, the equations of elastic-plastic constitutive law coupled with isotropic damage can be written as follows:

- elastic-plastic decomposition of the deviatoric part  $\dot{e}$  of the strain rate tensor  $\dot{\varepsilon}$  into an elastic part  $\dot{e}^e$  and a plastic part  $\dot{e}^{pl}$ :  $\dot{e} = \dot{e}^e + \dot{e}^{pl}$
- elastic law coupled with damage:  $\dot{s} = 2\mu(1-w)\dot{e}^e - \frac{\dot{w}}{1-w}s$
- *von Mises* yield function:  $f(s, r, w) = \frac{1}{1-w} \sqrt{\frac{3}{2}s : s} - \sigma_0(r)$
- plastic flow:  $\dot{e}^{pl} = \frac{3\lambda^{pl}}{2(1-w)^2\sigma_0(r)}s$  ,  $r = (1-w)\bar{\varepsilon}$  ,  $\lambda^{pl} = (1-w)\dot{\bar{\varepsilon}}$

where  $\sigma_0(r)$  represents the isotropic hardening law,  $\mu$  is the second Lamé parameter,  $\lambda^{pl}$  is the plastic multiplier and  $s$  is the spherical part of the stress tensor.

Numerical integration of these nonlinear equations is widely discussed in the next section.

### 2.3 Mixed velocity-pressure formulation

Let's consider a structure belonging to a domain  $\Omega \subset \mathbb{R}^d$ , where  $d$  is the spatial dimension. For  $d = 2$  plane strain hypothesis is considered. The structure is loaded with a displacement applied at the boundary  $\Gamma^1 \subset \partial\Omega$ , and a load is applied on the complementary part  $\Gamma^2$ . Due to plastic deformation incompressibility the mechanical problem has been formulated as a system of equations with two unknowns, velocity and pressure fields. Using the velocity vector  $v$  and the pressure scalar  $p$ , the conservation equations, for large elastic-plastic strain coupled with damage, can be expressed as follows:

$$\begin{cases} \operatorname{div}(s) - \nabla p = 0 \\ -\operatorname{div}(v) - \frac{1}{\chi(1-w)}\dot{p} - \frac{\dot{w}}{\chi(1-w)^2}p = 0 \end{cases} \quad (4)$$

where  $\chi$  is the bulk modulus.

The mixed velocity-pressure formulation for this problem takes the following form: find  $(v, p) \in V \times L^2(\Omega)$  such that:

$$\begin{cases} \int_{\Omega} s(v) : \dot{\varepsilon}(u) - \int_{\Omega} p \operatorname{div}(u) = \int_{\partial\Omega} (\sigma n) \cdot u \quad \forall u \in V^0 \\ - \int_{\Omega} q \operatorname{div}(v) - \int_{\Omega} q \left( \frac{1}{\chi(1-w)}\dot{p} + \frac{\dot{w}}{\chi(1-w)^2}p \right) = 0 \quad \forall q \in L^2(\Omega) \\ V = \{v \in (H^1(\Omega))^3; v = v^0 \text{ on } \Gamma^1\}, V^0 = \{v \in (H^1(\Omega))^3; v = 0 \text{ on } \Gamma^1\} \end{cases} \quad (5)$$

where  $\dot{\varepsilon}(u) = \frac{1}{2}(\nabla u + (\nabla u)^T)$

A stabilized discretization  $P1^+/P1$  has been considered to define the interpolation spaces. This finite element belongs to the family of mini-element initially used in the stokes equations [3]. This is a first order element with a linear continuous interpolation of both the pressure and the velocity fields, and also an enrichment of the velocity interpolation by a linear bubble function at the center of each finite element. This bubble function is used to ensure the stability condition [14]. The degrees of freedom associated to the bubble function are not linked to any other degree of freedom than those of the element, which allows to eliminate them at the element level. Therefore, this condensation procedure leads to a discrete global problem having the same degrees of freedom without bubble functions.

The computation scheme of the global problem is based on an incremental updated Lagrangian description. Due to the nonlinear elastic-plastic damage constitutive law, the finite element method leads to a nonlinear system of equations, which is solved using a Newton-Raphson algorithm. For each iteration, the equations are linearized and a correction is computed to improve the current estimate of the solution. The reader is referred to [11] where exhaustive details of this resolution are given.

## 3 Integration of constitutive equations

This section describes the numerical integration of the elastic-plastic damage constitutive equations (section 2.2) in an incremental computation procedure. Knowing the values  $(\dot{e}_n^p, w_n, s_n)$  at  $t_n$  and given a strain rate increment  $\dot{e}_{n+1}$  corresponding to the interval  $[t_n, t_{n+1}]$ , the numerical integration has to determine the updated values at the end of the interval,  $(\dot{e}_{n+1}^p, w_{n+1}, s_{n+1})$ .

The Newton-Raphson method has been combined with the radial return algorithm to achieve this integration.

At each Newton's iteration, a classical two-step method consisting of elastic predictor and plastic corrector has been applied. We start by testing a purely elastic evolution, then we check whether the trial yield stress lies inside of the trial yield surface. If this is true, the elastic trial state coincides with the updated state at  $t_{n+1}$ , and there is neither plastic flow nor damage evolution during the increment. Otherwise, the radial return method allows to determine the updated state at  $t_{n+1}$ .

A discretization of the constitutive equations, using the Euler implicit numerical scheme, leads to the following system of equations:

$$\begin{cases} s_{n+1} = \frac{s_n + 2\mu(1 - w_{n+1})\Delta t \dot{\epsilon}_{n+1}}{1 + \left( \frac{3\mu\Delta t \lambda_{n+1}^{pl}}{(1-w_{n+1})\sigma_0} + \frac{\Delta t \dot{w}_{n+1}}{1-w_{n+1}} \right)} \\ s_{n+1} : s_{n+1} = \frac{2}{3}(1 - w_{n+1})^2 \sigma_0^2 (r_{n+1}) \\ w_{n+1} - w_n = \Delta t \dot{w}_{n+1} \\ \lambda_{n+1}^{pl} = (1 - w_{n+1}) \dot{\bar{\epsilon}}_{n+1} \end{cases} \quad (6)$$

The unknowns of the system are  $s_{n+1}$ ,  $w_{n+1}$  and  $\lambda_{n+1}^{pl}$  (or  $\dot{\bar{\epsilon}}_{n+1}$ ). By injecting the first equation in the second we obtain the following system of equations:

$$\boxed{\begin{cases} (1 - w_{n+1} + \Delta t \dot{w}_{n+1})\sigma_0(r_{n+1}) + 3\mu\Delta t \lambda_{n+1}^{pl} - B_0 = 0 \\ w_{n+1} - w_n = \Delta t \dot{w}_{n+1} \end{cases}} \quad (7)$$

where  $B_0^2 = \frac{3}{2} s_{n+1}^T : s_{n+1}^T$  and  $s_{n+1}^T = s_n + 2\mu(1 - w_{n+1})\Delta t \dot{\epsilon}_{n+1}$  is the trial deviatoric stress.

By substituting some variables, the following system can be obtained, which has two unknowns i.e. plastic strain rate and damage:

$$\boxed{\begin{cases} f_1 = \left( 1 - w_{n+1} + \Delta t \left( \frac{-Y_{n+1}}{S_0} \right)^b \dot{\bar{\epsilon}}_{n+1} \delta_{\{\bar{\epsilon}_{n+1} \geq \bar{\epsilon}_d\}} \right) \sigma_0(r_{n+1}) + 3\mu(1 - w_{n+1})\Delta t \dot{\bar{\epsilon}}_{n+1} - B_0 = 0 \\ f_2 = w_{n+1} - w_n - \Delta t \left( \frac{-Y_{n+1}}{S_0} \right)^b \dot{\bar{\epsilon}}_{n+1} \delta_{\{\bar{\epsilon}_{n+1} \geq \bar{\epsilon}_d\}} = 0 \end{cases}} \quad (8)$$

where  $Y_{n+1} = \frac{-\sigma_0^2(r_{n+1})}{6} + \frac{-p_{n+1}^2}{2k(1-w_{n+1})^2}$ ,  $r_{n+1} = (1 - w_{n+1})(\dot{\bar{\epsilon}}_n + \Delta t \dot{\bar{\epsilon}}_{n+1})$

This system (with unknowns  $w_{n+1}$  and  $\dot{\bar{\epsilon}}_{n+1}$ ) is nonlinear. The Newton-Raphson procedure has been used for its resolution. Then the plastic multiplier can be obtained by  $\lambda_{n+1}^{pl} = (1 - w_{n+1})\dot{\bar{\epsilon}}_{n+1}$ . Finally, the deviatoric stress is given by:

$$s_{n+1} = \frac{s_n + 2\mu(1 - w_{n+1})\Delta t \dot{\epsilon}_{n+1}}{1 + \left[ \frac{3\mu\Delta t \lambda_{n+1}^{pl}}{(1-w_{n+1})\sigma_0} + \frac{\Delta t \dot{w}_{n+1}}{1-w_{n+1}} \right] \delta_{\{\lambda_{n+1}^{pl} > 0\}}} \quad (9)$$

### 3.1 Integration algorithms with different levels of coupling

The efficiency of numerical integration of the constitutive equations has a direct impact on the overall efficiency of the finite element approximation. As a result, the use of more complex

constitutive models can potentially involve a drastic increase in terms of computation time. To deal with this issue, three integration algorithms with different levels of coupling between damage and elastic-plastic behavior are studied here. These couplings are defined as follows:

1. The first one is called **strong coupling**: it consists in solving the nonlinear system (8) considering the two unknowns (damage and generalized strain rate) for each element and at each Newton-Raphson iteration.
2. The second one is called **intermediate coupling**: the system (8) is reduced to a nonlinear single equation where the unknown is the generalized strain rate. The damage value corresponding to the previous iteration is used to simplify the system. Then the new damage value is obtained using the second equation once the new generalized strain rate has been computed.
3. The third one is called **weak coupling**: it is similar to the intermediate coupling except that the damage value is not updated at each Newton-Raphson iteration but only at each time step of the incremental resolution.

### 3.2 Consistent tangent operator

To solve the nonlinear mechanical system, it is required to compute the deviatoric tangent operator, i.e.  $\frac{\partial s}{\partial \dot{\varepsilon}}$  in the mixed velocity pressure formulation (section 2.3). Simo et al. [27] have highlighted the importance of using a tangent operator consistent with the integration scheme used for the constitutive law.

$$L = \frac{\partial s_{n+1}}{\partial \dot{\varepsilon}_{n+1}} = \frac{\partial s_{n+1}}{\partial \dot{\varepsilon}_{n+1}} \frac{\partial \dot{\varepsilon}_{n+1}}{\partial \dot{\varepsilon}_{n+1}} = \frac{\partial s_{n+1}}{\partial \dot{\varepsilon}_{n+1}} (I_4 - I_2 \otimes I_2) \quad (10)$$

where  $(I_4)_{ij,kl} = \delta_{ik}\delta_{jl}$ ,  $(I_2 \otimes I_2)_{ij,kl} = \delta_{ij}\delta_{kl}$

After several derivations and simplifications, the final expression is given by:

$$L = \Delta t \left[ 2\mu(1 - w_{n+1})^2 \frac{\sigma_0}{B_0} (I_4 - \frac{1}{d} I_2 \otimes I_2) - \delta_{\{\lambda^{pl} > 0\}} 2\mu c s_{n+1} \otimes s_{n+1} \right] \quad (11)$$

where

$$c = \left( \frac{3\mu\lambda_{n+1}^{pl} + \sigma_0\dot{w}_{n+1}}{2B_0\lambda_{n+1}^{pl}} - \frac{3\mu\Delta t\lambda_{n+1}^{pl}}{2B_0\sigma_0} \frac{\partial\sigma_0}{\partial r} \right) \left( \frac{3\lambda_{n+1}^{pl}}{3\mu\sigma_0\lambda_{n+1}^{pl} + (B_0 - 3\mu\Delta t\lambda_{n+1}^{pl})\lambda_{n+1}^{pl} \frac{\partial\sigma_0}{\partial r} + \sigma_0^2\dot{w}_{n+1}} \right)$$

A deviatoric tangent bubble matrix is also needed to solve the mechanical problem. This matrix corresponds to the linear part of (11) [11]:

$$L^b = \Delta t \left[ 2\mu(1 - w_{n+1})^2 \frac{\sigma_0}{B_0} (I_4 - \frac{1}{d} I_2 \otimes I_2) \right] \quad (12)$$

### 3.3 Resolution algorithm

Let us consider the  $i^{th}$  Newton-Raphson iteration. The velocity  $v_i$  and therefore the strain rate  $\dot{\varepsilon}(v_i)$  are known. The following operations are performed at the next iteration:

- calculate  $\dot{e} = \dot{\varepsilon}(v_i) - \frac{1}{d}tr\dot{\varepsilon}(v_i)I$
- calculate  $B_0^i = \sqrt{\frac{2}{3}[s_n + 2\mu\Delta t(1 - w_{n+1}^{i-1})\dot{\varepsilon}_{n+1}^i] : [s_n + 2\mu\Delta t(1 - w_{n+1}^{i-1})\dot{\varepsilon}_{n+1}^i]}$
- apply an elastic predictor and a plastic corrector:
  - if  $(1 - w_{n+1}^i)\sigma_0(r_{n+1}^{i-1}) > B_0^i$  the increment is assumed purely elastic:  
 $\dot{\varepsilon}_{n+1}^i = 0$  and  $w_{n+1}^i = w_{n+1}^{i-1}$
  - otherwise, apply the plastic-damage corrector:  
calculate  $\dot{\varepsilon}_{n+1}^i$  and  $w_{n+1}^i$ .
- calculate the plastic multiplier  $\lambda_{n+1}^{pl} = (1 - w_{n+1}^i)\dot{\varepsilon}_{n+1}^i$
- evaluate  $s_{n+1}^i$ ,  $L_i$  and  $L_i^b$  by their expressions (9), (11) and (12);
- finally, knowing  $s_{n+1}^i$ ,  $L_i$  and  $L_i^b$   
 $p_{n+1}^{i+1}$  and  $v_{n+1}^{i+1}$  are obtained by solving the mechanical problem.

This process is iterated until convergence of the Newton-Raphson algorithm.

## 4 Non-local damage model

The straightforward finite element implementation of the standard damage formulation leads to mesh dependent results. The localization phenomenon occurs in very small areas and premature cracks onset can arise when the mesh is refined. Therefore, mesh refinement does not ensure convergence towards a physical solution. Many enhanced models have been proposed to overcome this deficiency and various numerical solution strategies have been developed [2, 4, 13, 15, 19, 20, 23, 28]. The non-local implicit gradient formulation [28] is one of these regularization methods, it has been employed in this study.

In order to describe correctly the localization phenomenon regardless spatial discretization, the non-local damage model introduces a non-local damage variable  $\bar{w}(x)$  to reflect the degree of material's degradation into the constitutive law. This non-local variable is considered as a weighted average of the standard damage variable  $w$ . Moreover, a new characteristic length parameter  $l_c$  is introduced to determine the size of the surrounding volume that effectively contributes to the non-local variable.

The gradient implicit formulation is obtained using a well-chosen weight function and the Taylor expansion. This leads to the following equations:

$$\begin{cases} -l_c^2 \Delta \bar{w} + \bar{w} = w & \text{in } \Omega \\ \nabla \bar{w} \cdot \vec{n} = 0 & \text{on } \partial\Omega \end{cases} \quad (13)$$

where  $\vec{n}$  is the unit outward normal to the external boundary  $\partial\Omega$ .

Non-local damage variable  $\bar{w}$  is implicitly related to the local damage variable  $w$  (13). Moreover,  $l_c^2$  acts as a diffusion term in this equation, and this parameter has a much greater influence on the size of localization areas than the mesh size does. Unfortunately, so far the physical definition of this characteristic length is not straightforward when dealing with metals [16].

The characteristic material length  $l_c$  corresponds to the grains average dimensions [22], or it is sometimes defined as the mean distance between micro-particles. In practice, it is usually

identified at the same time as the other material parameters. The inverse analysis approach is widely used in this identification of material parameters. In addition, some additional conditions have to be considered when choosing this characteristic length. For example, it is generally recommended to have  $l_c > h$ , where  $h$  is the mesh size, when the implicit gradient formulation with the non-local damage model are used.

The system of equations (13) has been solved by a linear finite element approximation. The obtained non-local damage variable  $\bar{w}$  substitutes to the standard damage variable  $w$  in the coupling with the behavior law.

## 5 Numerical results

Numerical examples presented in this section have two main focuses. The first one is to analyze the three integration algorithms with different levels of coupling of damage with the elastic-plastic behavior. The second one is to illustrate the effectiveness of the implicit gradient formulation with a non-local damage variable to ensure an objective damage analysis in our finite element approach.

Let's consider a rectangular plane plate submitted to a tensile test as depicted in figure 1. The contact between the tools and the specimen has been chosen as bilateral sticking (no decohesion and no tangential displacement). A vertical displacement  $u = 0.88 \text{ mm}$  has been imposed. Loading time  $T = 0.88 \text{ s}$  has been divided in uniform time steps,  $\Delta t = 0.005 \text{ s}$ . The material parameters of an aluminum alloy have been used:  $E = 70000 \text{ MPa}$ ,  $\nu = 0.3$ ,  $\bar{\epsilon}_d = 0$ ,  $w_c = 0.98$ ,  $b = 1$ ,  $s_0 = 1.25 \text{ MPa}$ , and  $\sigma_0(r) = 596(10^{-4} + r)^{0.31} \text{ MPa}$ .

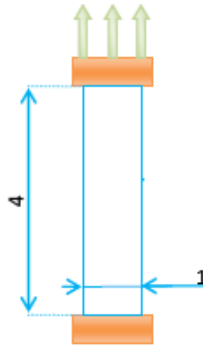


Figure 1: Geometry (mm) and boundary conditions

### 5.1 Numerical analyses of the three levels of coupling

Let's consider a uniform triangular mesh with a mesh size  $h = 0.12 \text{ mm}$ . Figure 2 shows load-displacement curves obtained by the three levels of coupling. Damage variable versus plastic strain, at the center of the specimen, are depicted in figures 3 and 4.

Strong and intermediate couplings seem to conduct to similar results both in term of load versus displacement and damage versus plastic strain (figures 2-b and 3). On the contrary, one can notice a slight difference when the weak coupling is used; figure 4 shows that the weak coupling leads to slower damage evolution in comparison to the strong coupling. This induces a slower softening of the behavior at the end of the tensile test, and thus a slower drop of the

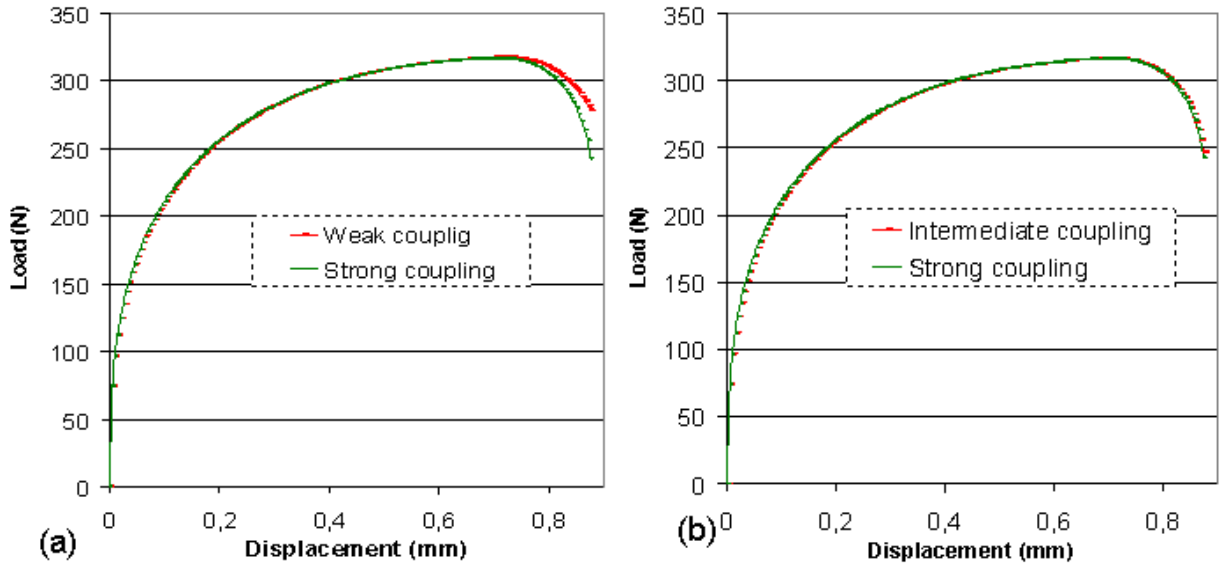


Figure 2: Load-displacement curves. (a) comparison between strong and weak couplings and (b) between strong and intermediate couplings.

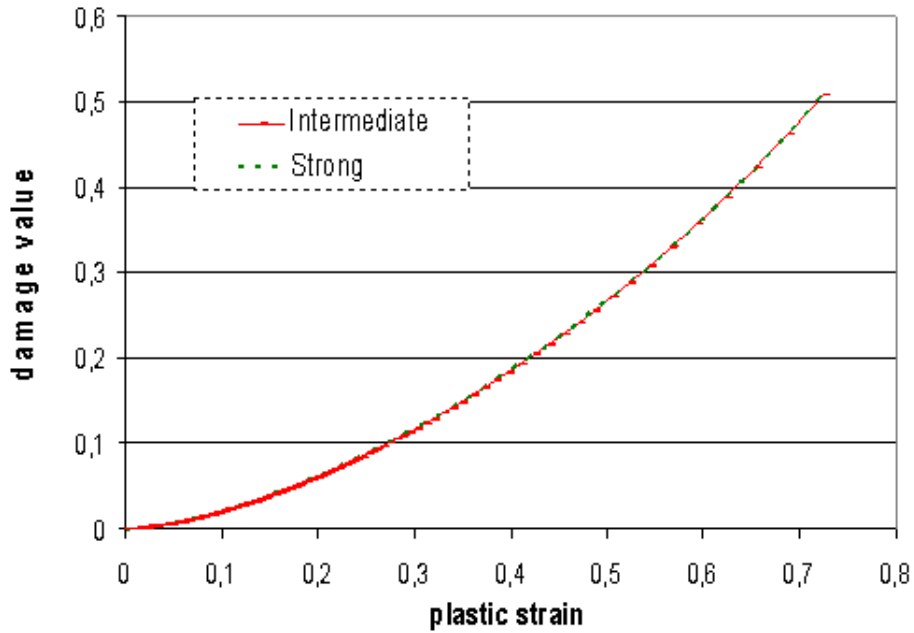


Figure 3: Damage evolution at the center of the specimen versus plastic strain: comparison between strong and intermediate coupling

load as shown in figure (2-a).

In order to assess results' sensitivity regarding time discretization, the same simulations were performed with two different time steps  $\Delta t_1$  and  $\Delta t_2$  and using the different levels of coupling. Figure 5 shows the load-displacement curves obtained for  $\Delta t_2 = \Delta t_1/2$ .

By using both strong and intermediate couplings, figures 5-a and 5-b show no sensitivity of the curves with respect to time discretization. On the contrary, the curves obtained using

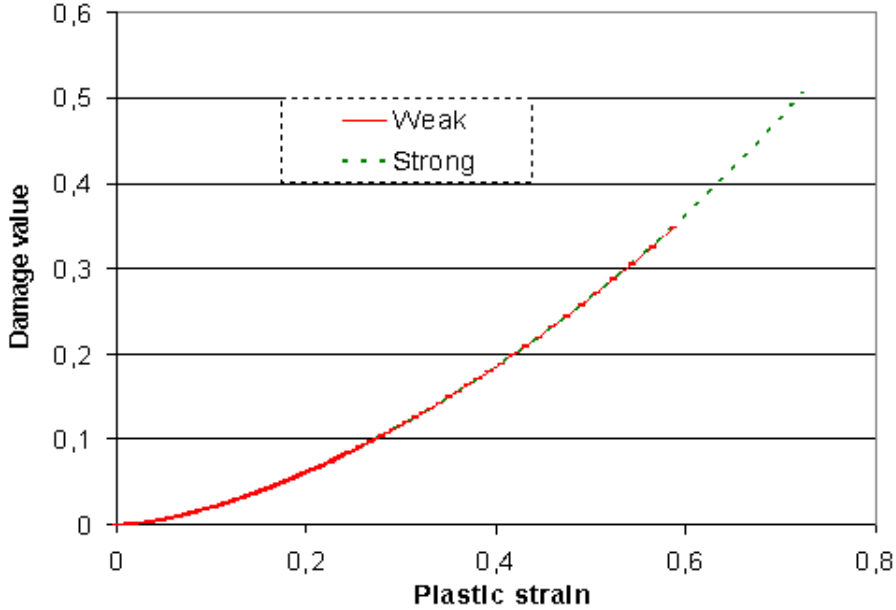


Figure 4: Damage evolution at the center of the specimen versus plastic strain: comparison between strong and weak coupling.

weak coupling depend on the time discretization, especially at the end of the simulation. This is due to softening phenomenon which develops at this stage and affects heavily load-displacement curves. To avoid this inconsistency, a fine time discretization is necessary at least in the late stage of damage growth when weak coupling is considered.

## Discussion

Weak coupling is sensitive to time discretization at the critical phase of the damage evolution. Indeed, updating the damage variable only at the end of each time increment is a simplifying assumption, which leads to an underestimation of the damage evolution when using a large time step. This is illustrated on load-displacement curve through a slower softening and a slower load drop when using the large time step  $\Delta t_1$ . The use of weak coupling requires therefore a time discretization as fine as possible particularly when the softening phenomenon is triggered.

Otherwise, weak coupling can be easily implemented in computational codes. It can be associated, without much difficulty, with the fracture modeling in the post critical stage of damage evolution. Moreover, it can reduce the cpu time due to the simplified method of updating the damage variable. This can lead to a lower influence upon convergence rate of mechanical problem, especially in the late stage of damage evolution.

Strong coupling requires a local integration at each element (when  $P^{1+}/P^1$  is used) of a nonlinear system with two unknowns. This involves a local integration of the constitutive law more expensive compared to the other levels of coupling where resolution of a single equation is required.

Intermediate coupling is considered as an alternative solution. It minimizes the drawbacks of the two other levels of coupling. Indeed, on the one hand, it simplifies the local integration of the constitutive law compared to the strong coupling. On the other hand, although it can lead

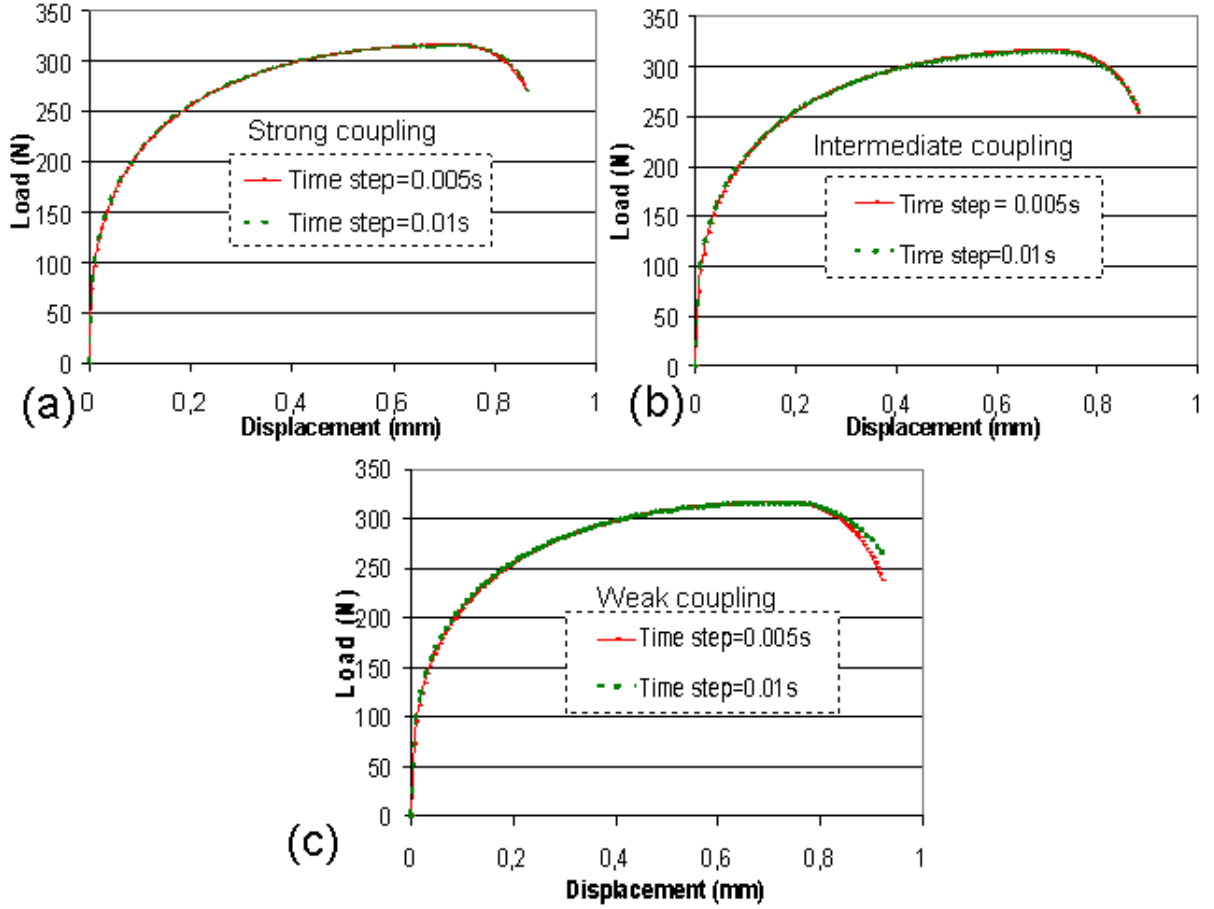


Figure 5: Load-displacement curves for two different time steps ( $\Delta t_1 = 1.10^{-2}s$ ) and ( $\Delta t_2 = 5.10^{-3}s$ ) for the three different levels of coupling.

to more computational cost than the weak coupling does, it provides a good approximation of the behavior law at each Newton-Raphson increment. Moreover, it is less sensitive to the time discretization and does not require a very fine time-step to allow an accurate integration of the constitutive law.

## 5.2 Numerical analyses of non-local damage model

In order to show the effectiveness of non-local damage model to regularize softening and localization phenomena as well as to reestablish results' objectivity in damage prediction analysis, the previous tensile test on a plane plate specimen has been used. Damage and plastic strain tend to localize in well-known shear bands in this test. Moreover, this numerical test is particularly useful to validate regularizing methods. Indeed, the load-displacement curves as well as the width of localization bands are very sensitive to the spatial discretization when the standard damage model is adopted.

Let's consider four uniform triangular meshes of the plate:  $h = 0.01mm$  (100454 elements),  $h = 0.02mm$  (24806 elements),  $h = 0.03mm$  (11137 elements),  $h = 0.04mm$  (6139 elements). The intermediate coupling, the previous material parameters and a characteristic material length  $l_c = 0.06mm$  have been also used to carry out simulations. Figure 6 depicts load-displacement

curves obtained by these different meshes.

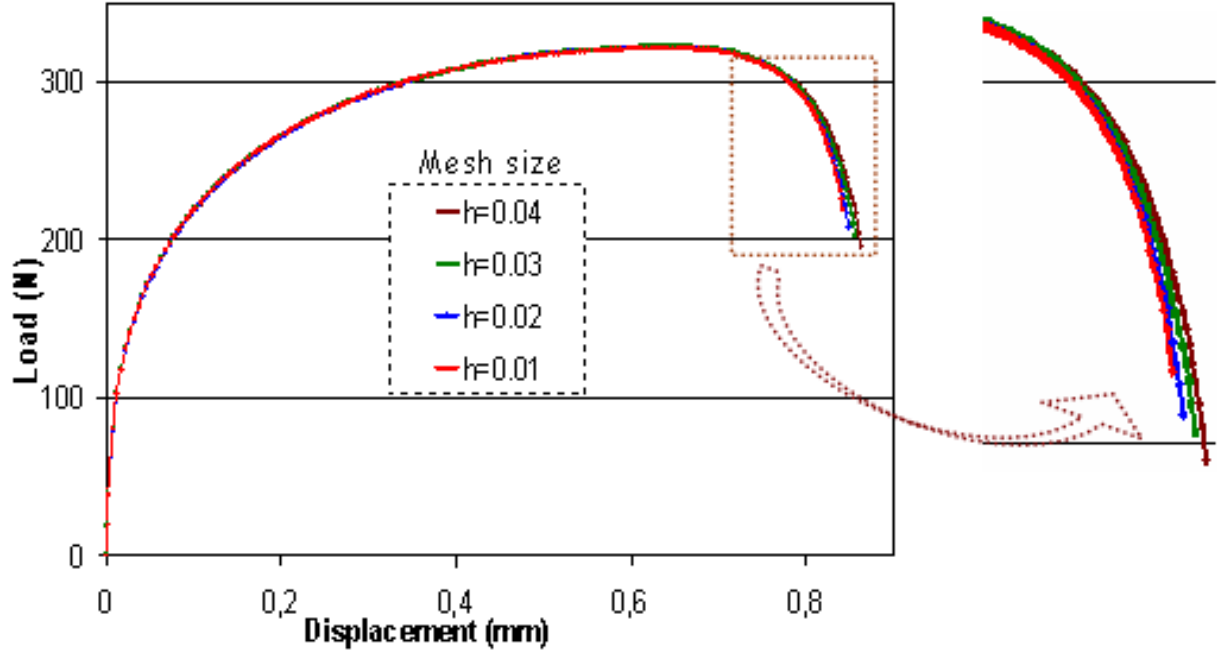


Figure 6: Load-displacement curves obtained with four different mesh sizes and the non-local damage model.

For each mesh, the load-displacement curve (figure 6) suggests that the elastic-plastic behavior is not influenced by damage at the beginning of the test. Beyond a given displacement value, a softening behavior is observed. This softening is due to the coalescence stage of microvoids and micro-cracks, and it leads to an important decrease of the structural strength of the material. Furthermore, when the mesh size decreases, curves tend toward the one obtained with the finest mesh. Therefore mesh convergence is attained.

Damage is the main cause of softening phenomenon in the elastic-plastic damage law. This softening is at the origin of the localization phenomenon, which leads to numerical results controlled by the spatial discretization when using the standard damage model. The isovalues of damage and plastic strain variables throughout the simulation, especially in the post critical stage and just before the macroscopic fracture, are also important indicators of the effectiveness of the regularization method.

Figures 7 and 8 present respectively damage and plastic strain isovalues for the four considered meshes. For each mesh size, the image presents the physical distribution of these fields: damage is localized at the center of the specimen and the plastic strain illustrates the formation of physical shear bands. Moreover, the shape and the size of these shear bands are not significantly influenced by the mesh size. This objective prediction is obtained thanks to the non-local damage model, which introduces a characteristic length to regularize the localization phenomenon.

In order to illustrate more clearly the non-local damage model effect on the size of localization areas and to see how different the results are in figure 8, figure 9 depicts line plots of plastic strain through the center cross-section of the specimen. This is the most damaged part of the plate wherein the steepest gradients occur.

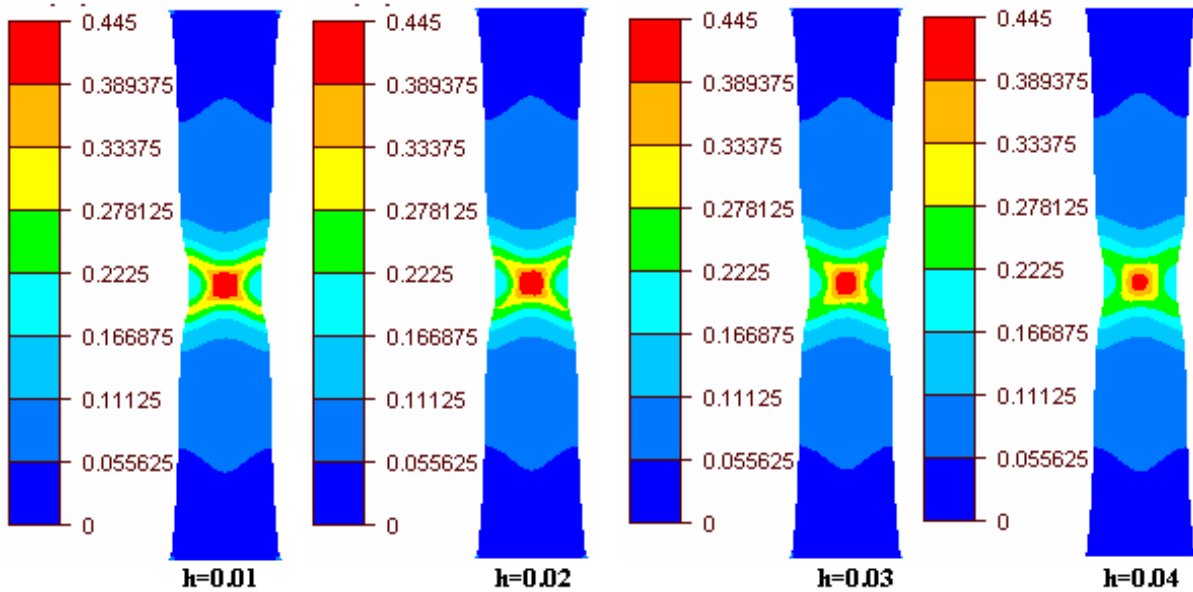


Figure 7: Damage isovalues for a vertical displacement  $u = 0.88 \text{ mm}$  for different values of mesh size  $h$ .

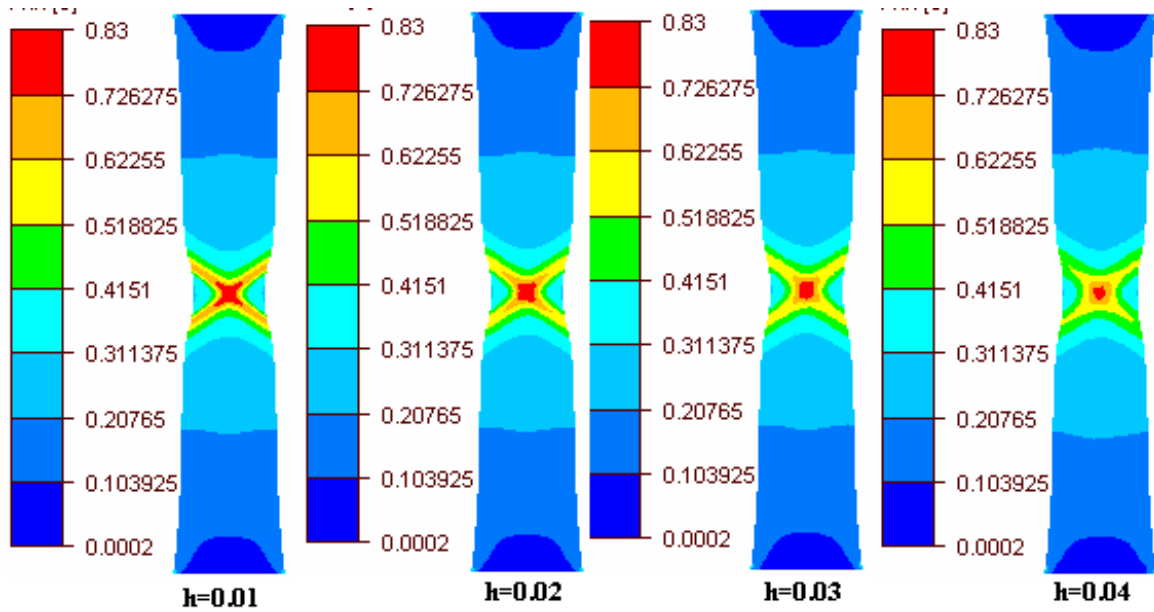


Figure 8: Plastic strain isovalues for a vertical displacement  $u = 0.88 \text{ mm}$  for different values of mesh size  $h$ .

Unlike standard damage model, where the plastic strain is generally highly localized in one element row, the localization zone of the plastic strain cannot be reduced to a strip of elements. Its size is thus different from the finite element size in the post-critical phase. In addition, we note that the amount of elements belonging to shear bands is getting lower when the mesh size increases (figure 9). First, this allows to avoid a unphysical, frank localization phenomenon when refining the mesh. Second, it enables to get a size of the shear bands less-sensitive regarding mesh size.

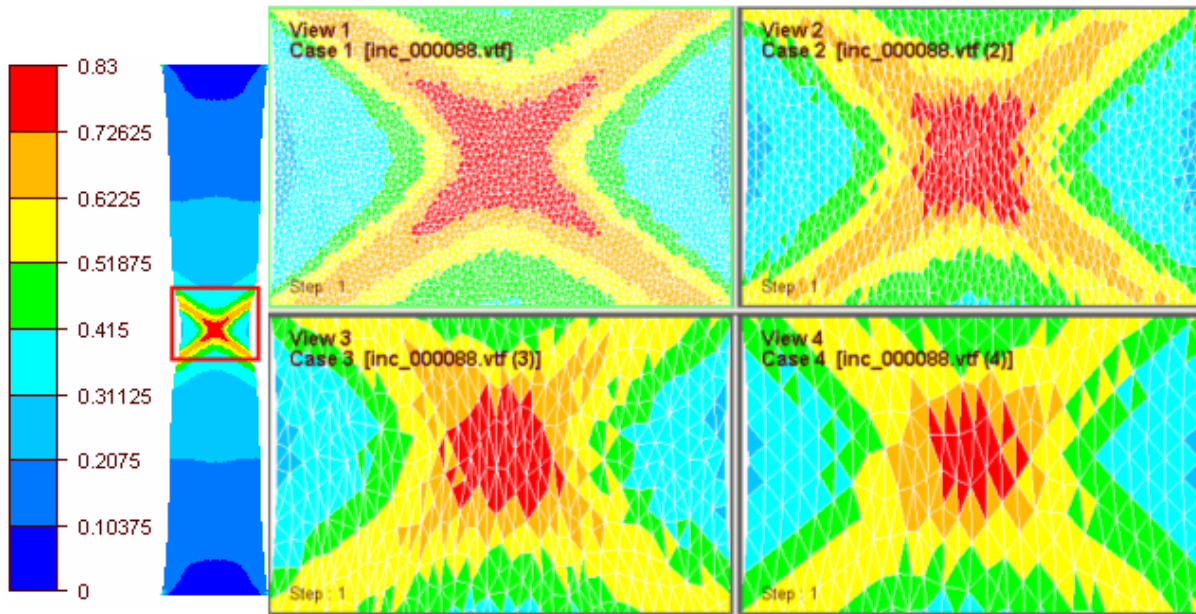


Figure 9: Center cross-section: plastic strain isovalues for a vertical displacement  $u = 0.88 \text{ mm}$  for different values of mesh size  $h$ .

It is also important to stress that this regularization model allows to ~~avoid~~ <sup>out</sup> premature fracture onset when using a very refined mesh. Mesh refinement is required to ensure reliable results for damage analysis, especially as mesh has to be refined enough around the localization areas in order to capture the locally steep gradient. Nowadays, adaptive mesh technique, which improves the accuracy without compromising the computation cost, is increasingly used for damage problems. However, adaptive mesh may lead to a severe mesh refinement in localization areas, therefore a premature fracture onset may occur when using a standard damage model. <sup>avoiding</sup>

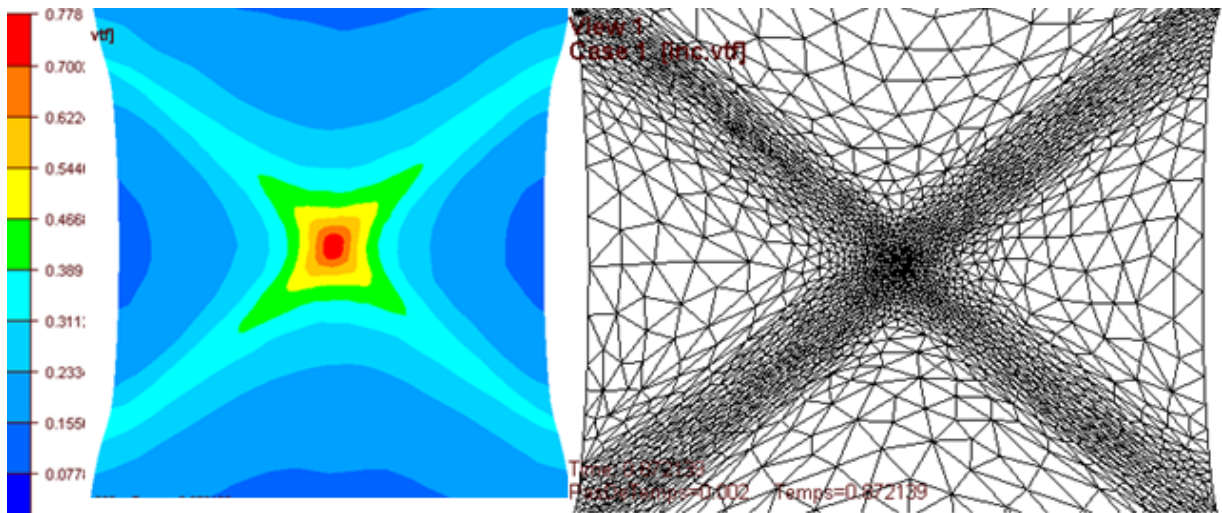


Figure 10: Center cross-section: mesh and line plots of damage for a vertical displacement  $u = 0.872 \text{ mm}$ .

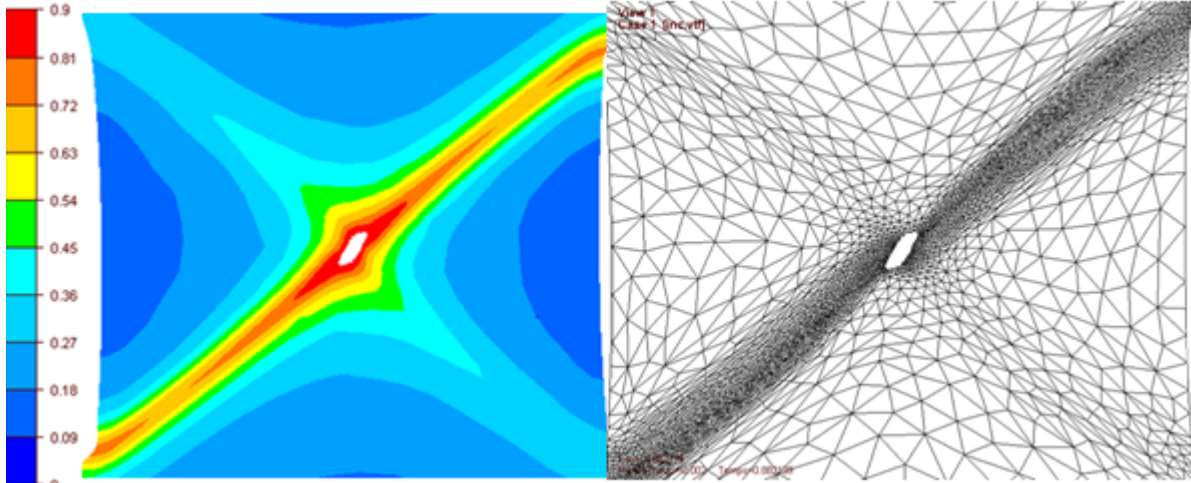


Figure 11: Center cross-section: mesh and line plots of damage for a vertical displacement  $u = 0.882 \text{ mm}$ .

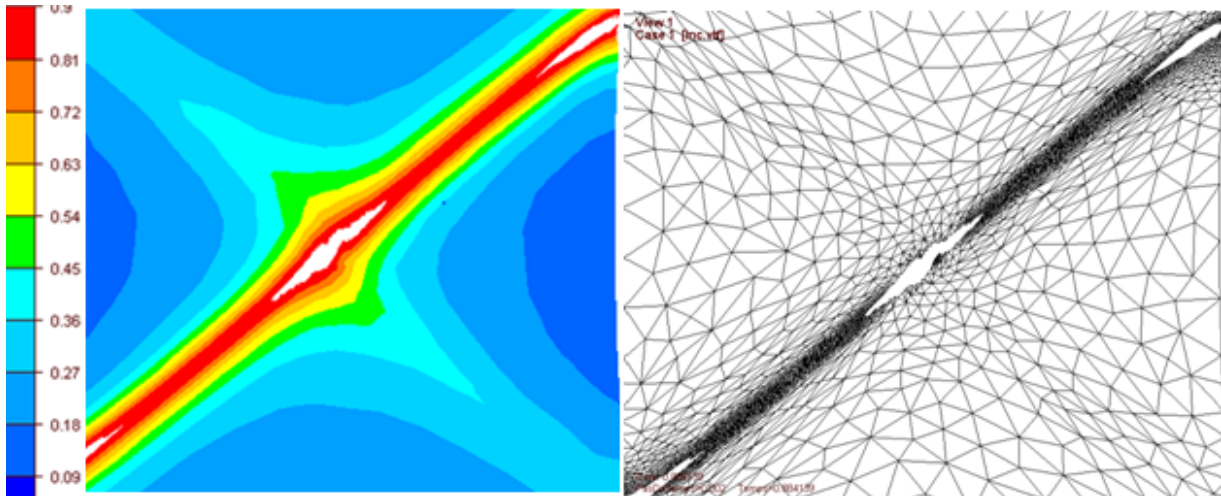


Figure 12: Center cross-section: mesh and line plots of damage for a vertical displacement  $u = 0.884 \text{ mm}$ .

Figures 10, 11 and 12 illustrate line plots of damage at the center cross-section along with the mesh evolution at the late stage of the previous simulation. An anisotropic mesh h-adaptation has been used to drive the mesh throughout the simulation, this mesh adaption relies on an error indicator based on the interpolation error estimate and taking into account  $w$  and  $\dot{w}$  variables [12]. The maximum and minimum mesh sizes have been respectively set ~~at~~ <sup>to</sup>  $h_{max} = 0.1\text{mm}$  and  $h_{min} = 0.005\text{mm}$ . Fracture has been modeled by the kill element method, i.e. when the damage variable  $w$  reaches the critical damage value  $w_c$  at one mesh element, this element is deleted from the mesh.

Figures 10, 11 and 12 show an anisotropic mesh around the localization areas. In addition, mesh elements are stretched in directions of low gradient of damage, and they are narrowed in directions of high gradient of damage in order to capture correctly the local steep gradient of damage. The non-local damage model is crucial in this case, indeed it enables to avoid a premature fracture onset when using a very small mesh size, which allows to conduct the

simulation till its latest stage.

Finally, macroscopic crack appears at the intersection of the two shear bands, then it propagates along one of the shear bands until the complete fracture of the plate. (Cette phrase j'hésite à l'enlever, qu'est ce que tu en pense? également je ne me suis pas trop tardé sur l'adaptation du maillage, car je pense que ça sort du framework)

tu peux garder cette phrase, et je rajouterai :

For more details about anisotropic mesh adaptation, the reader can refer to [12]

## 6 Conclusion

Numerical integration of an elastic-plastic damage constitutive law has been thoroughly addressed. This law is widely used in numerical modeling of materials processing involving large plastic strains together with the induced progressive degradation of material's properties.

To deal with the incompressibility of plastic deformation, a mixed velocity-pressure formulation and a stabilized finite element discretization  $P^{1+}/P^1$  have been used to solve the mechanical equations.

Three integration algorithms with different levels of coupling of damage with plastic strain have been presented and discussed. Intermediate coupling allows to simplify the constitutive law integration in comparison with the strong coupling. Moreover, although it is more difficult than the weak coupling, it provides a better approximation of the behavior law as well as of the damage evolution. Weak coupling can be easily implemented in computational codes and can lead to a less computational cost. However, a fine time discretization in the late stage of damage evolution is required in order to ensure an accurate integration of the constitutive law.

The finite element approximation of problems involving damage leads to numerical results severely sensitive to the spatial discretization. The implicit gradient formulation with a non-local damage variable, which introduces a characteristic material length to regularize the localization phenomenon, have been used to restore numerical results' objectivity.

Finally, tensile test on a plane plate specimen, where damage and plastic strain tend to localize in the well-known shear bands, has successfully proven both objectivity and effectiveness of the developed approach.

**Acknowledgments:** This study has been made with the support of the Technical Center for Mechanical Industries -CETIM- through an action on the numerical simulation of the mechanical joining processes in partnership with ARMINES.

## References

- [1] C. Agelet de Saracibar, M. Chiumenti, Q. Valverde, M. Cervera, On the orthogonal subgrid scale pressure stabilization of finite deformation J2 plasticity, *Comput. Methods Appl. Mech. Engrg.* 195 (2006) 1224–1251.
- [2] P.M.A. Areias, J.M.A. César de Sá, C.A.C. Antonio, A gradient model for finite strain elastoplasticity coupled with damage, *Finite Elem. Anal. Des.* 39 (2003) 1191–1235.
- [3] D.N. Arnold, F. Brezzi, M. Fortin, A stable finite element for stokes equations, *Calcolo* 21 (1984) 337–344.

- [4] Z.P. Bazant, M. Jirásek, Nonlocal integral formulations of plasticity and damage: survey of progress, *ASCE J. Engrg. Mech.* 128 vol. 11 (2002) 1119–1149.
- [5] Z.P. Bazant, G. Pijaudier-Cabot, Nonlocal continuum damage, localisation instability and convergence, *J. Appl. Mech.* 55 (1988) 287–293.
- [6] J.M.A. César de Sá, P.M.A. Areias, C. Zheng, Damage identification for anisotropic sheet-metals using a non-local damage model, *Int. J. Damage Mech.* 13 (2004) 35–57.
- [7] J.-L. Chenot, L. Fourment, K. Mocellin, Numerical treatment of contact and friction in FE simulation of forming processes, *J. Mat. Process. Techno.*, vol. 125-126, (2002) 45-52.
- [8] M. Chiumenti, Q. Valverde, C. Agelet de Saracibar, M. Cervera, A stabilized formulation for incompressible plasticity using linear triangles and tetrahedra, *Int. J. Plastic.* 20 (2004) 1487–1504.
- [9] D. Christ, A mixed finite element formulation for incompressibility using linear displacement and pressure interpolations, PhD thesis, ruhr-university bochum, Faculty for Civil Engineering, 2003.
- [10] S. Commend, A. Truty, T. Zimmermann, Stabilized finite elements applied to elastoplasticity: I. Mixed displacement-pressure formulation, *Comput. Methods Appl. Mech. Engrg.* 193 (2004) 3559–3586.
- [11] R. El khaoulani, Prédiction fiable de l’endommagement ductile par la méthode des éléments finis mixte : endommagement non local et adaptation de maillage. Thèse de doctorat, Ecole Nationale Supérieure des Mines de Paris, 2010.
- [12] R. El khaoulani, P.O. Bouchard, An anisotropic mesh adaptation strategy for damage and failure in ductile materials, *Finite Elem. Anal. Des.* 59 (2012) 1–10.
- [13] R.A.B. Engelen, M.G.D. Geers, F.P.T. Baaijens, Nonlocal implicit gradient-enhanced elasto-plasticity for the modelling of softening behaviour, *Int. J. Plast.* 19 (2003) 403–433.
- [14] M. Fortin, F. Brezzi, Mixed and hybrid finite element method, Springer Verlag, 1991.
- [15] M.G.D. Geers, R. Ubachs, R.A.B. Engelen, Strongly non-local gradient-enhanced finite strain elastoplasticity, *Int. J. Num. Meth. Eng.* 56 (2003) 2039–2068.
- [16] C. Iacono, L.J. Sluys, J.G.M. van Mier, Estimation of model parameters in nonlocal damage theories by inverse analysis techniques, *Comput. Methods Appl. Mech. Engrg.* 195 (2006) 7211–7222.
- [17] J. Lemaitre, J.L. Chaboche, *Mécanique des matériaux solides*, Dunod, Paris, 2001.
- [18] J. Lemaitre, R. Desmorat, *Engineering damage mechanics*, Springer, 2005.
- [19] T. Liebe, P. Steinmann, A. Benallal, Theoretical and computational aspects of a thermodynamically consistent framework for geometrically linear gradient damage, *Comput. Methods Appl. Mech. Engrg.* 190 (2001) 6555–6576.
- [20] B. Nedjar, Elastoplastic-damage modelling including the gradient of damage: formulation and computational aspects, *Int. J. Solids Struct.* 38 (2001) 5421–5451.

- [21] A. Needleman, Material rate dependence and mesh sensitivity in localization problems, *Comput. Methods Appl. Mech. Engrg.* 67 (1988) 69–85.
- [22] R.H.J. Peerlings, Enhanced damage modeling for fracture and fatigue, PhD thesis, Technische Universiteit Eindhoven, 1999.
- [23] R.H.J. Peerlings, R. de Borst, W.A.M. Brekelmans, M.G.D. Geers, Localisation issues in local and nonlocal continuum approaches to fracture, *Europ. J. Mech. A-Solids* 21 (2002) 175–189.
- [24] G. Pijaudier-Cabot, A. Huetta, Finite element analysis of bifurcation in nonlocal strain softening solids, *Comput. Methods Appl. Mech. Engrg.* 90 (1991) 905–919.
- [25] B. Ramesh, A.M. Maniatty, Stabilized finite element formulation for elastic-plastic finite deformations, *Comput. Methods Appl. Mech. Engrg.* 194 (2005) 775–800.
- [26] A. Rodriguez-Ferran, I. Morata, A. Huerta, Efficient and reliable nonlocal damage models, *Comput. Methods Appl. Mech. Engrg.* 193 (2004) 3431–3455.
- [27] J.C. Simo, R.L. Taylor, Consistent tangent operators for rate-independent elastoplasticity, *Comput. Methods Appl. Mech. Engrg.* 48 (1985) 101–118.
- [28] A. Suffis, T.A.A. Lubrecht, A. Combescure, Damage model with delay effect analytical and numerical studies of the evolution of the characteristic damage length, *Int. J. Solids Struct.* 40 (2003) 3463–3476.